DOI: 10.13009/EUCASS2023-989
Aerospace Europe Conference 2023 – 10TH EUCASS – 9TH CEAS

Robust Attitude Control Using Electrospray Thrusters

Gianni Pecora[⋆‡†], *Elisa Capello*[⋆], *Giuseppe Di Pasquale*[‡§] *and Manuel Sanjurjo-Rivo*[§]
[⋆]*Politecnico di Torino-C.so Castelfidardo, 39, 10129 Torino TO*
[‡]*IENAI SPACE - Av. Gregorio Peces Barba, 1, LeganÃ©s, 28919, Spain*
[§]*Universidad Carlos III de Madrid - Av.de la Universidad, 30, LeganÃ©s, 28919, Spain*
gianni.pecora@ienai.space · elisa.capello@polito.it · giuseppe.dipasquale@ienai.space · msanjurj@ing.uc3m.es
[†]Corresponding author

Abstract

Electrospray is a promising solution both for orbital control as primary propulsion, but also for spacecraft attitude control, acting as an actuator. This paper presents the study of attitude control of a spacecraft using an electrospray thruster-based attitude actuator. Robust controllers are explored, and different control laws algorithms have been tested. A study of the location and size of the actuators is performed as well, analyzing the impact on the performance of the controller in achieving and maintaining the desired attitude. The performance is evaluated in terms of power, propellant consumption and pointing error, showing how the robust controller can reject external disturbances and deal with model uncertainties.

1. Introduction

Electrospray technology is a promising electric propulsion solution that is becoming more popular for primary propulsion, especially for small satellites, thanks to its excellent performance in the low-power range. IENAI SPACE is developing ATHENA^{TM} (Adaptable THruster based on Electrospray for NAnosatellites) a modular electrospray thruster capable of adapting to the constraints coming from the other spacecraft subsystems and to meet the specific mission requirements. Alongside ATHENA^{TM}, IENAI is developing a suite of space mobility software tools, including GO^{TM} [5] and 360^{TM} by IENAI SPACE [6] (referred to as 360^{TM}), that can be used for advanced mission analysis and for defining the optimal ATHENA^{TM} configuration to fulfill a given mission. Jointly, it optimizes the associated low-thrust trajectories, which in turn generates requirements for the attitude control system, in terms of tracking and pointing accuracy with respect to the optimally defined guidance laws.

1.1 Problem

Over the years, there have been experimental demonstrations of the capabilities of electrospray thrusters, particularly their potential for precise attitude control and maneuverability [13,9]. However, these demonstrations have not provided specific details about the control strategies utilized. Instead, the emphasis has been on evaluating the achieved pointing accuracy under non-optimal control conditions and exploring their potential to replace or complement other attitude control mechanisms. The aim of this study is to identify an effective and robust control law to realize the optimal guidance trajectories derived from 360^{TM} tracking the desired optimal attitude. The controller shall ensure that the vehicle maintains the appropriate orientation even when there are external disturbances. ATHENA^{TM} Electrospray thrusters are used as attitude controllers, and this work explores the effectiveness of different control laws and the number of clusters to be used at different body positions. The position and velocity obtained, including the control and attitude dynamics, are then compared against the 360^{TM} mission analysis tool to determine the impact on the overall propulsion system performance. The simulation environment and the spacecraft subsystems are modeled in Matlab & Simulink.

1.2 Overview

In control theory, mathematical models are employed to describe closed-loop control systems that incorporate feedback, such as spacecraft control systems, and are effective in managing disturbances. This study examines several controller types, including the Proportional-Integral-Derivative (PID) control, which is a commonly used feedback algorithm. However, the PID control may not be suitable for non-linear or time-varying systems, since it cannot handle uncertainty.

DOI: 10.13009/EUCASS2023-989

Sliding Mode Control (SMC) is a robust method that utilizes a sliding surface to guide the system trajectory. This study explores Second-order Sliding Mode Control, which improves upon SMC by driving both the sliding variable and its derivative to zero. Additionally, Super-Twisting Sliding Mode Control (STSMC) is investigated, which ensures a zero sliding variable and reduced chattering. It is possible to identify the conditions that the sliding variable must satisfy to obtain globally and asymptotically closed-loop stability[10]:

$$\begin{aligned} \dot{V} &= \vec{\sigma}\dot{\vec{\sigma}} < 0 \\ \lim_{|\vec{\sigma}|\to\infty} V &= \infty \end{aligned} \tag{1}$$

where $\vec{\sigma}(x(t))$ is the sliding surface and V is a Lyapunov function, which can take many forms, and there are several methods to construct it depending on the specific properties of the system.

Electrospray thrusters

Micro-satellites like CubeSats have transitioned from educational tools to versatile platforms for commercial and research missions due to their low cost, flexibility and thanks to the advancements in the miniaturization of critical technologies. [12]. Consequently, to meet the strict constraints of small satellites, the demand for compact and efficient propulsion systems has grown. The electrospray technology is gaining significant interest due to the employment of an efficient mechanism that allows for the electrostatic acceleration of ionic liquid propellants. This allows to offer compact and scalable solutions, whose advantages include high efficiencies at low power, good specific impulse (1000 to 2000 s range) and relatively high thrust-to-power ratio. Additionally, the propellant is an inert liquid and the systems do not require an external cathode for ion neutralization. ATHENA^{TM}, a micro-fabricated electrospray thruster developed by IENAI SPACE [15], exemplifies these advantages and can easily adapt to mission requirements in terms of total impulse, while offering a lightweight, compact and low-power propulsion system.

2. Mathematical model

This work employs the following reference frames:

- Earth-Centered Inertial (ECI): origin at the center of the Earth. The $\hat{i}_{ijk}$ axis aligns with the vernal equinox, $\hat{k}_{ijk}$ extends through the North pole and $\hat{j}_{ijk}$ completes the right-hand triad.
- Radial-Circumferential-Normal (RCN) (also known as LVLH): origin at the spacecraft's center of mass. The $\hat{i}_{rcn}$ axis points from the center of the Earth to the spacecraft's center of mass, $\hat{k}_{rcn}$ is parallel to the orbital angular momentum and $\hat{j}_{rcn}$ completes the right-hand triad.
- Body reference frame: origin at the spacecraft's center of mass and the $\hat{i}_B$,$\hat{j}_B$,$\hat{k}_B$ vectors vary based on the mission, forming a right-handed system.

The rotation matrix for transforming vectors from ECI to body frame (DCM_{ECI2B}) can be derived using Euler's angles. However, singularities can occur and to address them, the use of quaternion (q) transformation matrices is a viable option. By rotating a fixed reference frame to any desired frame using an angle α around a single axis $\vec{a}$ (known as the Euler rotation axis), the transformation can be achieved: $DCM_{ECI2B} = f(q)$ [2].

2.1 Attitude Dynamics

The equation of motion for angular momentum ($\vec{h}$ can be written as $d\vec{h} = \vec{M}dt$, where $\vec{M}$ is the applied torque. Expressing the vectors in the body frame, we have $\dot{\vec{h}} + \vec{\omega}_B \times \vec{h}_B = \vec{M}_B$.
Using the inertia matrix J, Euler's equation of motion becomes:

$$\dot{\vec{\omega}}_B = J^{-1}(\vec{M}_B - \vec{\omega}_B \times J\vec{\omega}_B) \tag{2}$$

To describe the evolution of the body's attitude, we use quaternions, whose kinematics is described by the differential equation [2]:

$$\dot{q}_{B2ECI} = \frac{1}{2}\Omega(\vec{\omega}_B)q_{B2ECI} + K_{quat}(1 - (q_0^2 + q_1^2 + q_2^2 + q_3^2))q_{B2ECI} \tag{3}$$

DOI: 10.13009/EUCASS2023-989

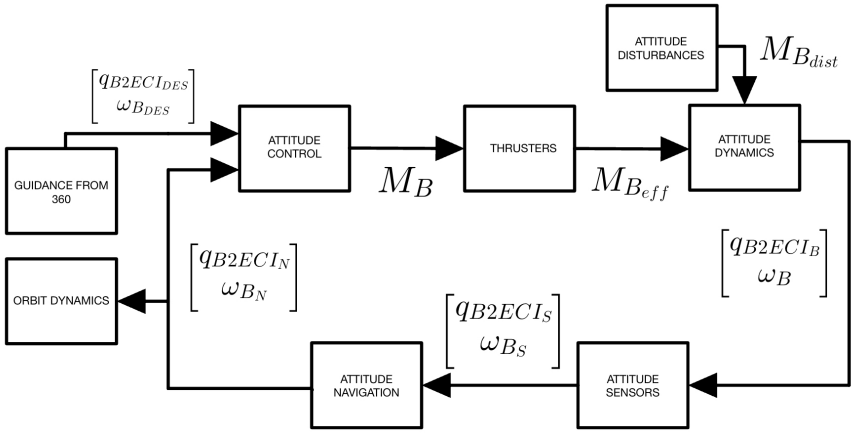

Figure 1: Outline of the model

The additional term $K_{quat}(1-(q_0^2+q_1^2+q_2^2+q_3^2))q_{B2ECI}$ accounts for the quaternion constraint $q_0^2+\vec{q}\cdot\vec{q}=1$, preventing constraint violation during numerical integration. $\Omega(\vec{\omega}_B)$ is defined as follow:

$$\Omega(\vec{\omega}_B)=\begin{bmatrix} 0 & -\omega_1 & -\omega_2 & -\omega_3 \\ \omega_1 & 0 & \omega_3 & -\omega_2 \\ \omega_2 & -\omega_3 & 0 & \omega_1 \\ \omega_3 & \omega_2 & -\omega_1 & 0 \end{bmatrix} \tag{4}$$

2.2 Attitude Disturbances

This work considers the following attitude disturbances:

- Earth's magnetic torque: it is described by the equation $\vec{M}_{M_B}=\vec{m}\times\vec{B}_B$, where $\vec{m}$ represents the magnetic residual dipole and $\vec{B}_B$ the magnetic induction, both in the body reference frame. The magnetic field is determined using the International Geomagnetic Reference Field (IGRF).
- Aerodynamic torque: in Low Earth Orbit (LEO), residual air molecules and atomic oxygen can cause drag, which needs to be modeled to control the spacecraft's attitude. The spacecraft's external surface can be divided into planar surfaces with outward unit normals ($\vec{n}_i$). The surface areas (A_i) and the velocity relative to the atmosphere in the body frame ($\vec{v}_{B_{rel}}$) are also taken into account. The aerodynamic torque on each surface is approximated as $\vec{M}_i=d_i\vec{n}_i\times-\frac{1}{2}C_D\rho(\vec{n}_i^T\vec{v}_{B_{rel}})\vec{v}_{B_{rel}}A_i$. The total aerodynamic torque $\vec{M}_{D_B}$ on the spacecraft is obtained by summing the torques of the individual surfaces [7].
- Gravity gradient torque: it arises from the non-uniform gravitational field in space. It is given by $\vec{M}_{GG_B}=3\mu|\vec{r}_B|^{-5}\vec{r}_B\times(J\vec{r}_B)$, where μ is the Earth's standard gravitational parameter, J is the inertia matrix, and $\vec{r}_B$ is the position vector in the body frame.

The total disturbances in the body frame are calculated as $\vec{M}_{B_{dist}}=\vec{M}_{M_B}+\vec{M}_{D_B}+\vec{M}_{GG_B}$. These disturbances significantly impact the spacecraft's attitude dynamics.

2.3 Attitude Navigation and Sensors

The following navigation sensors are considered:

- Star Tracker: this model utilizes angular accuracy and frequency data from a Star Tracker sensor's data sheet to determine q_{B2ECI_S} through quaternion multiplication.
- Micro Electro-Mechanical Systems (MEMS) gyroscope: this sensor is used to measure angular velocity. It can be modeled using the equations $\vec{\omega}_{B_S}=\vec{\omega}_B+b+na$ and $\dot{b}=n_b$. The white noise components n_a and n_b are defined using equations that involve parameters such as the Angle Random Walk (ARW) and Rate Random Walk (RRW), which can be obtained from the gyroscope data sheet. The model includes bias stability, bits, range, gyroscope frequency, and scale factor non-linearity as well [3].

DOI: 10.13009/EUCASS2023-989

In addition, the study incorporates a Discrete Multiplicative Quaternion Extended Kalman Filter for navigation. The Kalman Filter operates in a "predict-correct" loop, where it predicts the system state and uncertainty for the next time step and updates them based on measurements [14]. At the end of the process, the estimated quaternion q_{B2ECI_N} and the angular velocity ω_{B_N} are obtained.

2.4 Orbit Dynamics

ATHENA^{TM} electrospray thrusters are only impemented for attitude control. For orbit propagation, the system of first-order modified equinoctial orbital elements [16] is used, since it exhibits no singularity under certain conditions. Furthermore, the zonal gravitational perturbation caused by Earth's oblateness (described by the J_2 harmonic) is also included. Additionally, a main thruster is introduced for orbit control to compare its performance with the 360^{TM} software. Proper attitude control with electrospray thrusters ensures the correct pointing of the main thruster for executing optimized trajectories. The 360^{TM} software provides several pieces of information, including the time-varying attitude from the body to ECI in quaternions ($q_{B2ECI_{des}}$), the thrust vector of the main thruster in the body reference frame ($\vec{T}_{B_{MT}}$), the specific impulse of the main thruster ($I_{sp_{MT}}$) and the evolution of the trajectory, expressed either in cartesian or classical elements.. The acceleration in the body reference frame ($\vec{a}_B$) is determined by dividing the thrust vector by the spacecraft mass, which is time varying as well.

2.5 Guidance

The Guidance is composed of a time-varying quaternion $q_{B2ECI_{des}}$, provided by the space mobility tool 360^{TM}, to represent the attitude of the body reference frame with respect to the Earth-Centered Inertial reference frame. This guidance profile aims at achieving a specific maneuver, assuming that a main thruster is used for orbital control. The desired angular velocity $\vec{\omega}_{B_{des}}$, consistent with the attitude, is derived using transformation matrices:

$$\vec{\omega}_{B_{des}} = DCM_{ECI2B} DCM_{RCN2ECI}\, \vec{\omega}_{RCN2ECI_{RCN_{des}}} \tag{5}$$

In this equation, $\vec{\omega}_{RCN2ECI_{RCN_{des}}} = \begin{bmatrix} 0 & 0 & \frac{2\pi}{\hat{T}} \end{bmatrix}$ represents the desired angular velocity of the RCN reference frame relative to the ECI reference frame, measured in the RCN reference frame. The variable $\hat{T}$ represents the orbital period. On the other hand, DCM_{ECI2B} and $DCM_{RCN2ECI}$ are rotation matrices that allow transformation between different reference frames.

2.6 Thrusters

Electrospray thrusters consist of two parallel emitters that generate positive and negative ion beams for attitude control. The thrust produced by the emitters is determined by the voltage applied to them. The sum of the thrusts from the two emitters gives the total thrust vector $\vec{T}$. Each emitter's thrust is influenced by the voltage and three current components: nominal, spike and white-noise. Efficiency factors such as polydispersity (η_p), divergence (η_θ), and energy (η_E) are considered as well. The propellant consumption (m_i) and power consumption (P_i) of each emitter "i" are calculated based on the thrust and current values.
The orientation of the thrusters with respect to the spacecraft's body reference frame is modeled using in-plane and out-of-plane angles (α and β) that create a transformation matrix: $\vec{F}_B = A_{T2FB}\vec{T}$. The position of each resultant force $\vec{T}_i$ in the body reference frame is denoted as $\vec{r}_{T_i} = [r_{x_B}, r_{y_B}, r_{z_B}]$. The total torque generated by the forces is obtained by the following expression:

$$\begin{bmatrix} \vec{M}_{x_B} \\ \vec{M}_{y_B} \\ \vec{M}_{z_B} \end{bmatrix} = \begin{bmatrix} r_{T_1}(1) & r_{T_2}(1) & r_{T_3}(1) & r_{T_4}(1) & r_{T_5}(1) & r_{T_6}(1) & r_{T_7}(1) & r_{T_8}(1) \\ r_{T_1}(2) & r_{T_2}(2) & r_{T_3}(2) & r_{T_4}(2) & r_{T_5}(2) & r_{T_6}(2) & r_{T_7}(2) & r_{T_8}(2) \\ r_{T_1}(3) & r_{T_2}(3) & r_{T_3}(3) & r_{T_4}(3) & r_{T_5}(3) & r_{T_6}(3) & r_{T_7}(3) & r_{T_8}(3) \end{bmatrix} \times \begin{bmatrix} \vec{F}_{x_B} \\ \vec{F}_{y_B} \\ \vec{F}_{z_B} \end{bmatrix} \tag{6}$$

The torque obtained from attitude control ($\vec{M}_B$) can be transformed into the resultant force required for each pair of emitters using the inverse of the transformation matrix. Analogously, after deriving the effective thrust from the electrospray model, it is possible to calculate the effective torque in the body reference frame ($\vec{M}_{B_{eff}}$) for attitude dynamics.

DOI: 10.13009/EUCASS2023-989

3. Attitude control laws

Various control laws, such as PID and SMC, are estimed and tested. A method to evaluate control performance is proposed, which will be applied in a mission scenario example. The closed-loop control system uses attitude quaternion error as feedback ($q_e = \begin{bmatrix} q_{e_0} & \vec{q}_e \end{bmatrix}$), calculated using the conjugate of the desired quaternion and the estimed quaternion derived from navigation. The angular velocity error ($\vec{\omega}_e$) is computed as the difference between the desired and actual angular velocities.

3.1 Proportional-Integral-Derivative Control

The first control law analyzed is the Proportional-Integral-Derivative (PID) in a closed-loop quaternion feedback control. The following equation represents the PID control formulation:

$$\vec{M}_B = -K_I \int \vec{q}_e \text{sign}(q_{e_0}) dt - K_P \vec{q}_e \text{sign}(q_{e_0}) - K_D \vec{\omega}_e \tag{7}$$

Here, $\vec{M}_B$ represents the control input in the body reference frame, and K_I, K_P, and K_D are positive constants.

3.2 Super Twisting Sliding Mode Control

The Super Twisting Sliding Mode Control (STSMC) is a robust second-order control technique that utilizes a sliding surface derived from optimal-control analysis [4]. The following loss function must be minimized to determine the optimal switching surface:

$$\Pi(\omega) = \frac{1}{2} \int_{t_s}^{\infty} \left[\rho \vec{q}_e{}^T \vec{q}_e + \vec{\omega}_e^T \vec{\omega}_e \right] dt \tag{8}$$

where ρ is a scalar gain and t_s is the time of arrival at the sliding manifold.
To drive the system to the desired trajectory in the shortest possible path and to minimize Eq. (8) the following surface is chosen:

$$\vec{\sigma} = \vec{\omega}_e + c_1 sign(q_{e_0}) \vec{q}_e = 0 \tag{9}$$

where c_1 is a positive constant.
The control torque using quaternions feedback control is [10]:

$$\vec{M}_B = -\lambda |\vec{\sigma}|^{1/2} sign(\vec{\sigma}) + \vec{u}_1, \;\; \dot{\vec{u}}_1 = \begin{cases} -\vec{M}_B & |\vec{M}_B| > U_M \\ -\alpha sign(\vec{\sigma}) & |\vec{M}_B| \leq U_M \end{cases} \tag{10}$$

where α, U_M and λ are positive constants.

3.3 Variable Structure Sliding Mode Control

The Variable-Structure Sliding Mode Control (VSSMC) is implemented as well. This control mechanism is known for its robustness in dealing with uncertainties and requires knowledge of the inertia matrix for improved accuracy. The sliding surface is selected based on the quaternion error: $\vec{\sigma} = \vec{\omega}_e + c_1 sign(q_{e_0}) \vec{q}_e$. Considering Eq. (2) and setting $\dot{\vec{\sigma}} = 0$ the motion off the surface is prevented, causing the state trajectory to stay on the sliding manifold. The variable structure control with quaternion error, denoted as $q_e = \begin{bmatrix} q_{e_0} & \vec{q}_e \end{bmatrix}$, is obtained as follows [8]:

$$\vec{M}_B = J \left\{ \frac{c_1}{2} \left[|q_{e_0}| (\vec{\omega}_{B_{des}} - \vec{\omega}_{B_N}) - sign(q_{e_0}) \vec{q}_e \times (\vec{\omega}_{B_{des}} + \vec{\omega}_{B_N}) \right] + \dot{\vec{\omega}}_{B_{des}} - G\vec{s} \right\} + \vec{\omega}_{B_N} \times (J \vec{\omega}_{B_N}) \tag{11}$$

$$\vec{s} = \begin{cases} 1 & for \;\; \vec{\sigma} > \varepsilon \\ \vec{\sigma}/\varepsilon & for \;\; |\vec{\sigma}| \leq \varepsilon \\ -1 & for \;\; |\vec{\sigma}| < -\varepsilon \end{cases} \tag{12}$$

where G is positive definite and ε,c_1 are positive constants. A saturation function $\vec{s}$ is used to mitigate chattering caused by the discontinuous term.
The stability of the controller is demonstrated by verifying Lyapunov's equations (Eq. (1)) using a candidate Lyapunov

DOI: 10.13009/EUCASS2023-989

function: $V = 0.5 \cdot \vec{\sigma}^T \vec{\sigma} \iff \dot{V} = \dot{\vec{\sigma}}\vec{\sigma}$. Considering Euler's equation (Eq. (2)), Eq. (11) and the sliding surface $\vec{\sigma}$ the following expression is obtained:

$$\dot{V} = -\vec{\sigma}^T G \vec{s} \tag{13}$$

which is always less or equal to zero as long as G is positive definite, demonstrating asymptotic stability.
The robustness of the VSSMC is addressed by considering modeling errors and external disturbances [4]. The error in the inertia matrix and the disturbance input are defined, and their effects on the sliding surface derivative are analyzed. It is shown that the system remains robust to these uncertainties and disturbances.

3.4 Dynamic Super Twisting Sliding Mode Control

The Dynamic Super Twisting Sliding Mode Control (DSTSMC) is computed using the same sliding surface of the previous SMC and its control input $\vec{M}_B$ is the sum of STSMC and VSSMC. Therefore, by summing the equations, the following formulation is obtained:

$$\vec{\sigma} = \vec{\omega}_e + c_1 sign(q_{e_0})\vec{q}_e \tag{14}$$

$$\vec{M}_B = \vec{u}_D + \vec{u} \tag{15}$$

$$\vec{u}_D = J\left\{\frac{c_1}{2}\left[|q_{e_0}|(\vec{\omega}_{B_{des}} - \vec{\omega}_{B_N}) - sign(q_{e_0})\vec{q}_e \times (\vec{\omega}_{B_{des}} + \vec{\omega}_{B_N})\right] + \dot{\vec{\omega}}_{B_{des}} - G\vec{s}\right\} + \vec{\omega}_{B_N} \times (J\vec{\omega}_{B_N}) \tag{16}$$

$$\vec{s} = \begin{cases} 1 & for\ \ \vec{\sigma} > \varepsilon \\ \vec{\sigma}/\varepsilon & for\ \ |\vec{\sigma}| \leq \varepsilon \\ -1 & for\ \ |\vec{\sigma}| < -\varepsilon \end{cases} \tag{17}$$

$$\vec{u} = -\lambda|\vec{\sigma}|^{1/2} sign(\vec{\sigma}) + u_1, \quad \dot{u}_1 = \begin{cases} -\vec{M}_B & |\vec{u}| > U_M \\ -\alpha sign(\vec{\sigma}) & |\vec{u}| \leq U_M \end{cases} \tag{18}$$

where G is positive definite and ε,α, λ,c_1 are positive constants.
This controller is the sum of two robust controllers and thus provides more flexibility. The DSTSMC also considers that the constants change over time with respect to q_e to ensure both accuracy and control authority when needed.

3.5 Performance evaluation

A method to evaluate the performance of each controller is explained considering 4 different parameters: Rise Time (R), Maximum Overshoot (O), Steady State Error (S) and Propellant Consumption (M). The efficiency of each parameter is evaluated as a percentage using the method shown in Table 1. A maximum error constraint (e_{max}) of 1° is imposed and m_{max} represents the mass of propellant used with thrusters always on.

Table 1: Evaluation of performances

R=100 % R=0 %	Very fast response Very slow response	$R = \frac{T_{period}/2 - Rise\_Time}{T_{period}/2} \times 100\%$
O=100 % O=0 %	No Overshoot Very high Overshoot	$O = \frac{\pi - Max\_Overshoot}{\pi} \times 100\%$
S=100 % S=0 %	No Steady-State Error Steady-State Error equal to the maximum error required	$S = \frac{e_{max} - e_{steady\_state}}{e_{max}} \times 100\%$
M=100 % M=0 %	Thrusters always off Thrusters always on	$M = \frac{m_{max} - m_{propellant}}{m_{max}} \times 100\%$

The error e(t) for this evaluation is considered in terms of Euler's angles derived from the error quaternion q_e.
The performance of the above-mentioned attitude control methods is analyzed. The case study considers a circular Sun-synchronous orbit at an altitude of 567 km. Initially, the orbital elements are given in Table 2 and the orbital

a [km]	e	i [rad]	ω [rad]	Ω [rad]	ν [rad]
6938	0	1.7043	0	3.5952	0

Table 2: Orbital elements at time zero

period is calculated as 1.5976 hours.

DOI: 10.13009/EUCASS2023-989

A 6U Cubesat is considered, with dimensions $0.34065 \times 0.1 \times 0.2263$ [m] and mass $m = 7.98$ kg. Different guidance laws (such as steps of different amplitude) and thrusters configurations are analyzed after a fine-tuning phase. An example of guidance, that makes the spacecraft move in a sinusoidal way, is presented in Figure. 2 in terms of quaternions $q_{B2ECI_{des}}$ in order to illustrate the differences in performance beetween the previously control laws.

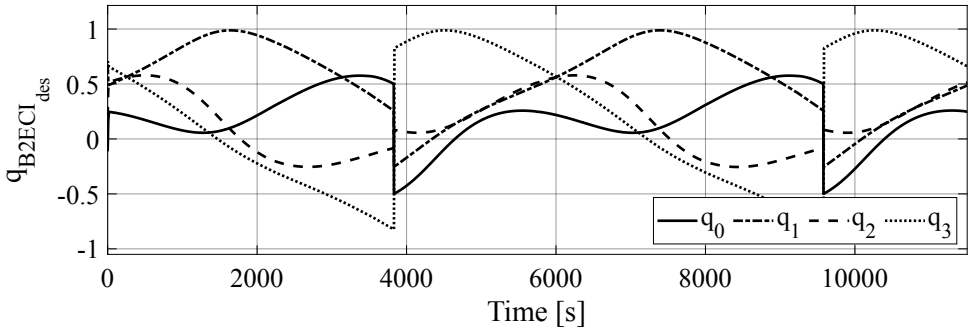

Figure 2: Trend of quaternions $q_{B2ECI_{des}}$

Figure. 3 shows the locations of resultant forces for each pair of emitters: the thrusters T_1, T_3, T_6, T_8, operate in the z_B direction and have an inclination angle of 0 degrees. On the other hand, T_2, T_4, T_5, T_7 operate in the x_B direction and have an inclination angle of 10 degrees. In order to determine the best control law, the simulation was conducted

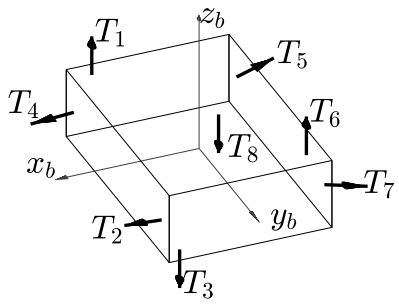

Figure 3: 6U Cubesat with 8 pairs of emitters

using all the different control laws that were previously analyzed. The performance of each control law was evaluated, and the results, in terms of angular errors, are presented in Table 3. It can be observed that despite the minimal propellant consumption, the implementation of a PID controller leads to significant overshoots and steady-state errors. Conversely, both STSMC and VSSMC demonstrate improved outcomes. In fact, the overshoots are reduced compared to the previous scenario. The most favorable performance is observed when utilizing DSTSMC. To better compare how all 4 control laws perform, a new parameter, called Efficiency, is introduced in order to summarize the four metrics:

$$Efficiency = \frac{mean(R_\Psi, R_\theta, R_\Phi) + mean(O_\Psi, O_\theta, O_\Phi) + mean(S_\Psi, S_\theta, S_\Phi) + M}{4} \tag{19}$$

It considers the average Euler angles over the three parameters R, O and S (rise time, maximum overshoot and steady-state error) to which propellant consumption is added. In Figure. 4 can be seen that, although the propellant consumption is a bit high, the most efficient control law is the DSTSMC. As mentioned earlier, this is an exhaustive example that also reflects cases with different control laws. The analysis of two different mission scenarios that will be done in the next section will exclusively use this control law.

DOI: 10.13009/EUCASS2023-989

Table 3: Performance comparison of the different controllers

PID Performance Evaluation				
Ψ	99.3 %	97.85 %	91.94 %	96.58 %
θ	97.82 %	74.08 %	68.25 %	
Φ	93.76 %	92.22 %	44.38 %	
	R	**O**	**S**	**M**
STSM Performance Evaluation				
Ψ	99.72 %	99.95 %	93.97 %	97.83 %
θ	97.24 %	97.95 %	85.62%	
Φ	99.96 %	99.84 %	73.44 %	
	R	**O**	**S**	**M**
Variable Structure SM Performance Evaluation				
Ψ	99.47 %	99.91 %	94.65 %	98.57 %
θ	97.1 %	86.89 %	83.51 %	
Φ	99.6 %	99.83 %	69.84 %	
	R	**O**	**S**	**M**
Dynamic STSM Performance Evaluation				
Ψ	99.92 %	99.85 %	96.6 %	96.93 %
θ	94.33 %	99.33 %	92.77 %	
Φ	99.96 %	99.82 %	84.08 %	
	R	**O**	**S**	**M**

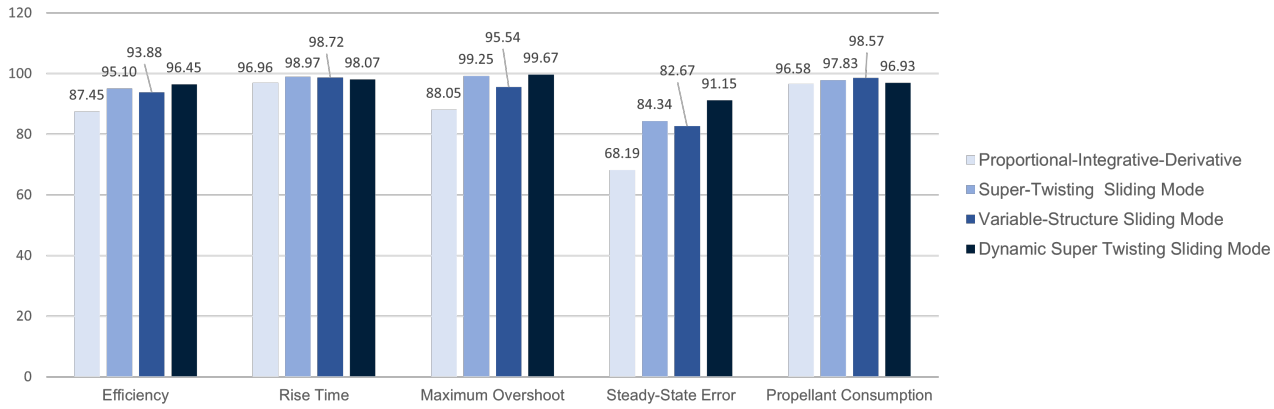

Figure 4: Performance Efficiency

4. Results

Two different mission scenarios involving electrospray thrusters are considered. The analysis takes into account the position and number of thrusters in each scenario. By comparing the results of these analyses, it is possible to gain a deeper understanding of the performance and effectiveness of electrospray propulsion systems in various mission scenarios.

For both mission scenarios, it is considered the same micro-satellite equipped with two deployable solar panels. The dimensions of the micro-satellite are $0.3 \times 0.227 \times 0.4$ [m] and it has a mass of 48 kg.

The two mission scenarios aim to reach different orbits using the attitude control provided by ATHENA^{TM} electrospray thrusters, allowing the main thruster to be steered in the right direction with constant thrust. From this point on, a single thruster is considered as the sum of two emitters: each $\vec{T}_i$ represents the resultant force of two emitters with opposite polarity. Figure. 5 illustrate two distinct configurations of Electrospray thrusters within the micro-satellite. The first configuration exhibits only six thrusters situated along the y and z body directions, enabling easier control over the satellite's attitude. Conversely, the second configuration features only eight pairs of emitters, known as thrusters, positioned at various locations in y and z body directions. Furthermore, a red vector denotes the placement and orientation of the main thruster. Considering the data sheets given, a model of star tracker [1] and gyroscope [11] are

DOI: 10.13009/EUCASS2023-989

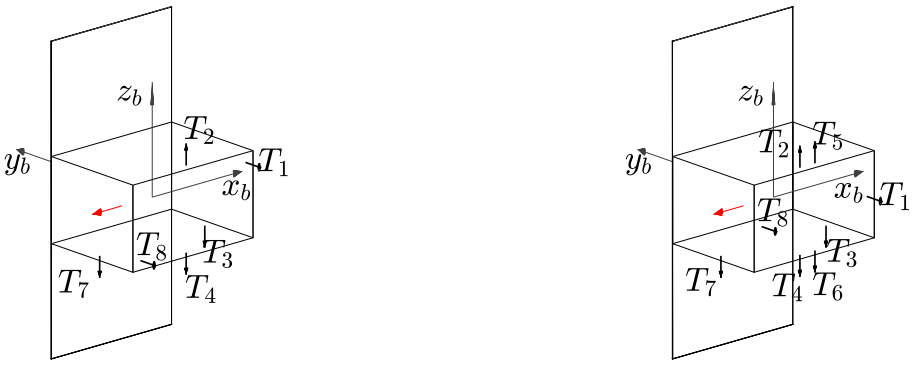

Figure 5: Two different configurations of Electrospray thrusters on a microsatellite

implemented. Table 4 shows the initial orbital elements. The orbit is nearly circular with a small eccentricity value (e

a [km]	e	i [rad]	ω [rad]	Ω [rad]	ν [rad]
6937	0.005978	1.7071	4.844	3.5953	1.4386

Table 4: Orbital elements at time zero

$\simeq 0$). The simulated attitude disturbances are applied to the micro-satellite during seven orbits, taking into account the initial time parameters discussed earlier. The solar panel is included as an additional surface to emulate atmospheric drag, although it does not accurately replicate the real scenario due to the presence of shadowing effects.

4.1 Mission Scenario 1

In the first scenario, the goal is to reach a different orbit thanks to the main thruster. The attitude control must ensure that the main thruster points in the right direction during the phase called "thrust pointing". This scenario spans over

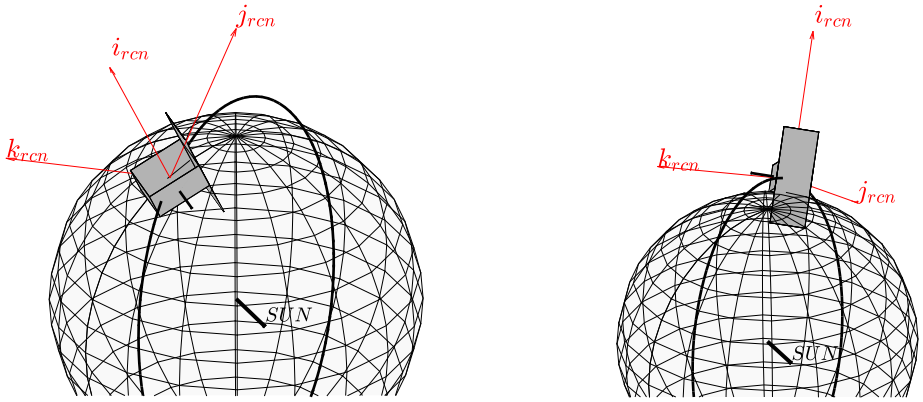

Figure 6: Thrust pointing at two different times, highlighting the change in orientation of the satellite throughout the orbit

seven orbital revolutions and consists of a single phase, whose pointing mode is referred to as "thrust pointing". 360^{TM} mission analysis tool provides the desired quaternions $q_{B2ECI_{des}}$. This trajectory causes the satellite to move in an oscillatory pattern, which aims at modifying the inclination, and two views in time of how it moves in the orbit are shown in Figure. 6. This figure shows the spacecraft, the orbit, the Sun's direction and the main thruster's direction.

DOI: 10.13009/EUCASS2023-989

The electrospray thrusters are not visible in the figure.
Results for the two configurations (Figure. 5) are presented and compared. Quaternions for 4 periods of time and a zoom of them (Figure. 7) show that there is an oscillation only in the first orbital period and that it is lower in the case with 8 thrusters. If the performance is considered from the perspective of the angular error, the same trend is obtained (Figure. 8): oscillations in the first orbital period of 2 and 1 degree (respectively for 6 and 8 thruster configurations), and after that, the control matches closely the desired attitude. Considering the thruster effort in the first two time

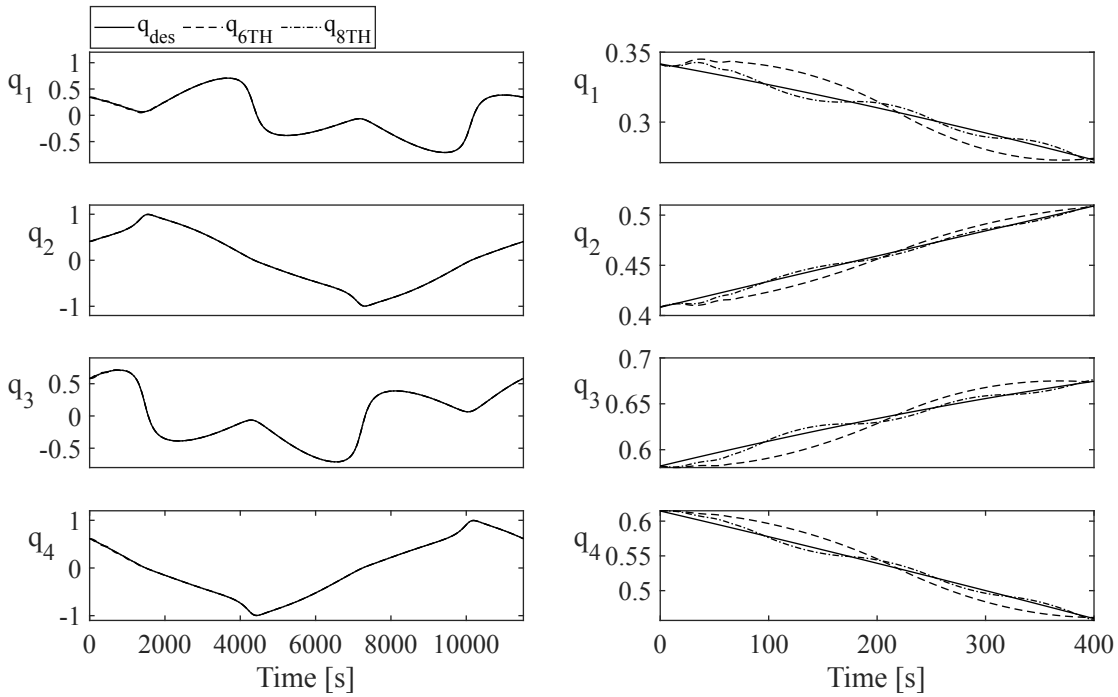

Figure 7: Quaternions during the first 4 orbital periods (left) and a detail in the first 400 seconds (right), showing desired and results for both considerations considered

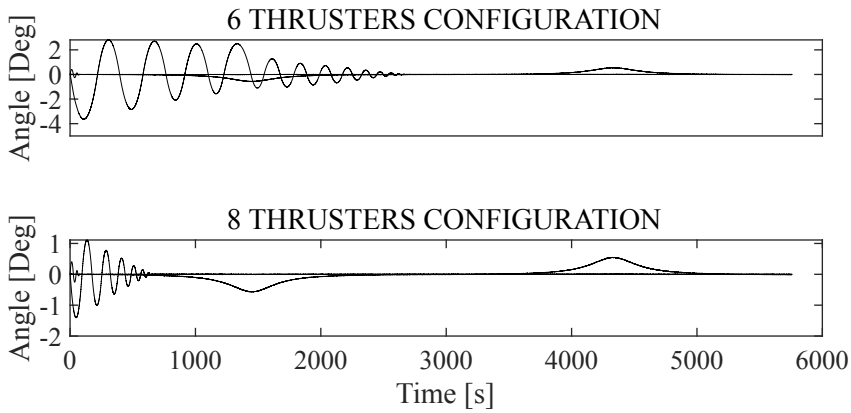

Figure 8: Angular error during the first 6000 seconds

periods, the configuration for each thruster and the case with 8 and 6 pairs of emitters is shown in Figure. 9. In both cases, the effort of thrusters 1 and 8 is less for two main reasons: they act on creating a moment in z but most of the rotations occur in the other two directions; they are also located far from the center of mass and therefore greater moments are obtained with lower forces. The same figure displays the sustained power consumption for 8 and 6 pairs of emitters. Furthermore, To provide a clearer understanding of the behavior, the moving average of each thruster and power consumption is represented in a red trend. Figure. 9 also showcases the amount of propellant required over time. The dotted line indicates the propellant in the case where all emitters are always turned on at maximum thrust. Comparing the two configurations, is possible to observe that the use of 6 thrusters saves 0.1 grams of propellant.

DOI: 10.13009/EUCASS2023-989

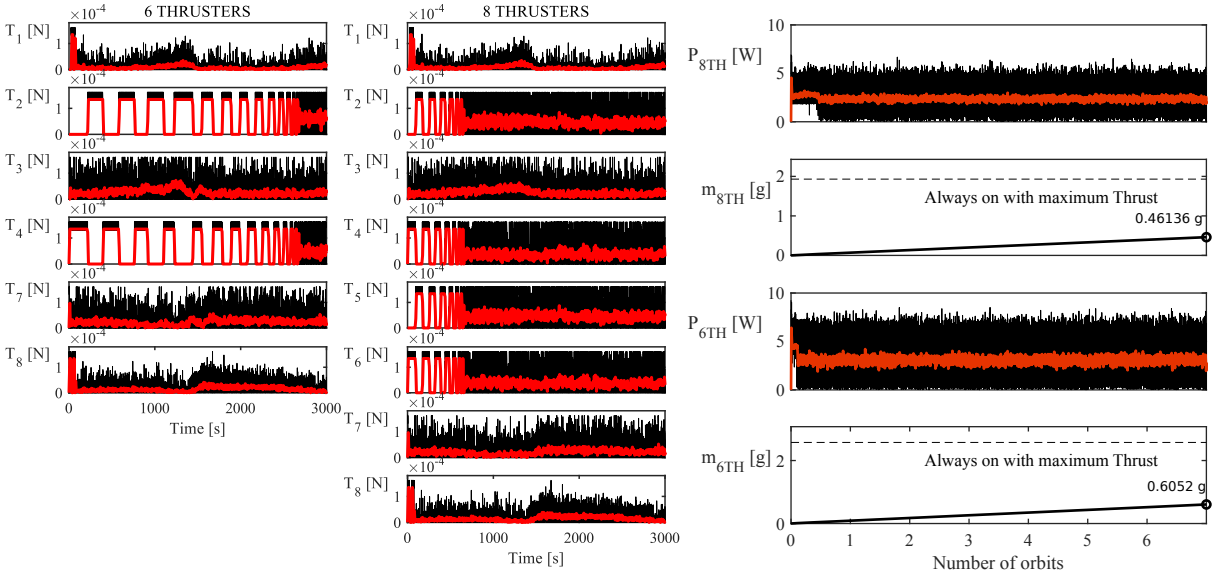

Figure 9: Effort of the thrusters considering the configuration with 6 and 8 pairs of emitters (left). Propellant and total power consumption for both configurations (right)

Position and velocity error with respect to 360^{TM} by IENAI Space is shown in Figure. 10. Considering control with 8

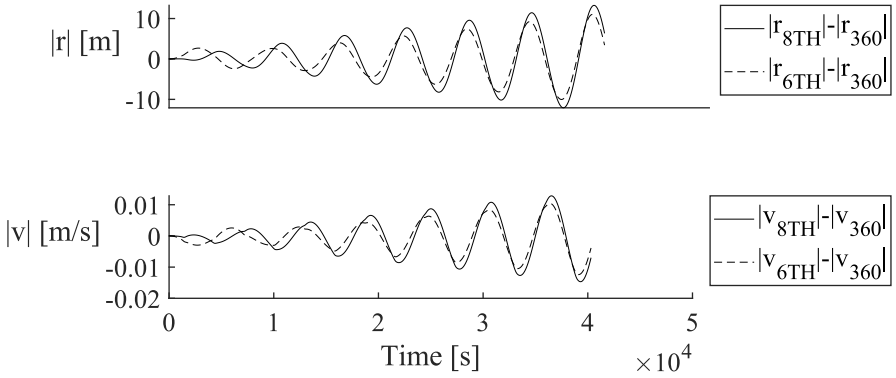

Figure 10: Error in position and velocity compared with those provided by the 360^{TM} mission analysis tool

and 6 thrusters, there is a position difference of a few meters. It is interesting to observe how, in the case where there are no sudden phase changes, after an initial oscillation, control allows for extremely low tracking errors. The expected final trajectory is reached with a difference of a few meters (about 10 meters from 360^{TM}). Depending on the final accuracy or propellant savings, one or the other configuration can be chosen. In fact, using 6 thrusters saves propellant, but at the expense of a little more error in position.

4.2 Mission Scenario 2

The second mission scenario is composed of some phases and three different modes: thrust pointing, sun-pointing and communication. These modes alternate during 7 orbits.
The objective of this scenario is to see how the attitude control performs in different possible real phases. In addition, the main thruster is turned on only in the thrust pointing phase. Unlike the previous scenario, there are mode changes and rise time must be minimized in the transition from one phase to another. The thrust pointing phases are the same as in the previous scenario (Figure. 6); while different views of the sun-pointing and communication phases are shown, respectively, in Figure. 11 and Figure. 12.

DOI: 10.13009/EUCASS2023-989

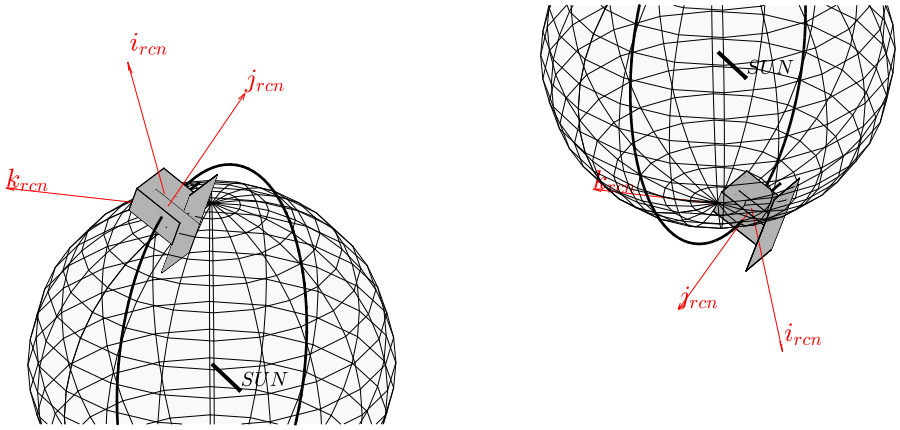

Figure 11: Sun pointing during time

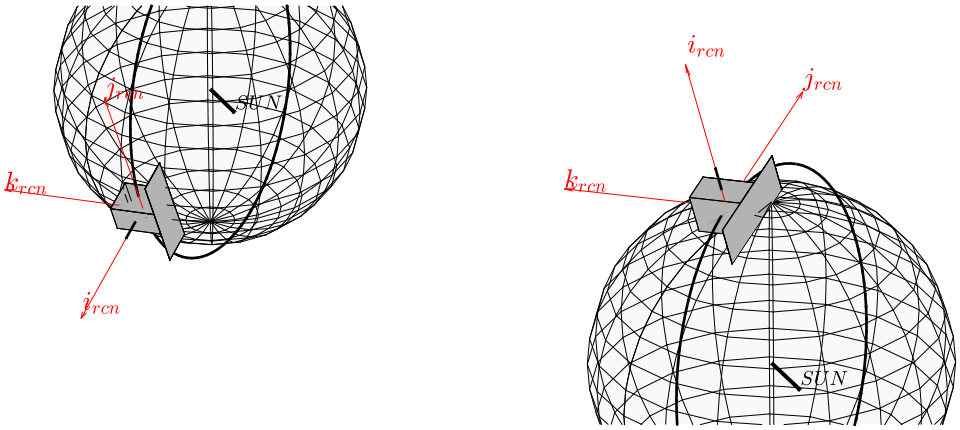

Figure 12: Communication mode during time

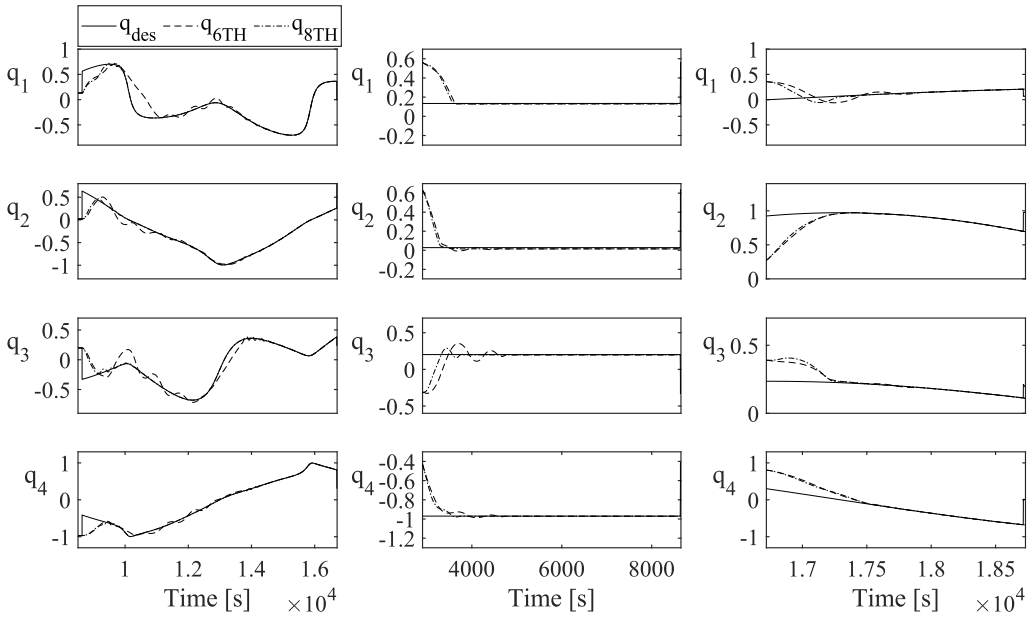

Figure 13: Quaternions during thrust pointing (left) sun-pointing (center) and communication (right) phases. The two configurations are both compared with the desired quaternions

DOI: 10.13009/EUCASS2023-989

In the thrust pointing phases, we can see an initial phase of oscillation, relevant in the case of 6 Thrusters. In fact, in Figure. 13, it can be seen that in the transition from the previous phase, the quaternions approach the desired ones after a certain amount of time. The same trend could be observed if angular errors were used, which show that at the end, it is possible to achieve a steady state error on the magnitude order of $10^{-3}[^{\circ}]$. Effort of the thrusters are the same as in the previous scenario.
In the sun-pointing mode, the objective is to recharge the solar panel and thus have a fixed attitude in the direction of the sun. In fact, the desired quaternions are constants (Figure. 13). It is possible to observe that, as before in switching from one phase to another, there is an initial oscillation and then a steady state error. Oscillation is slightly higher when 6 thrusters are used. In this case, the effort of the thrusters is shown in Figure. 14 and the red trend represents their

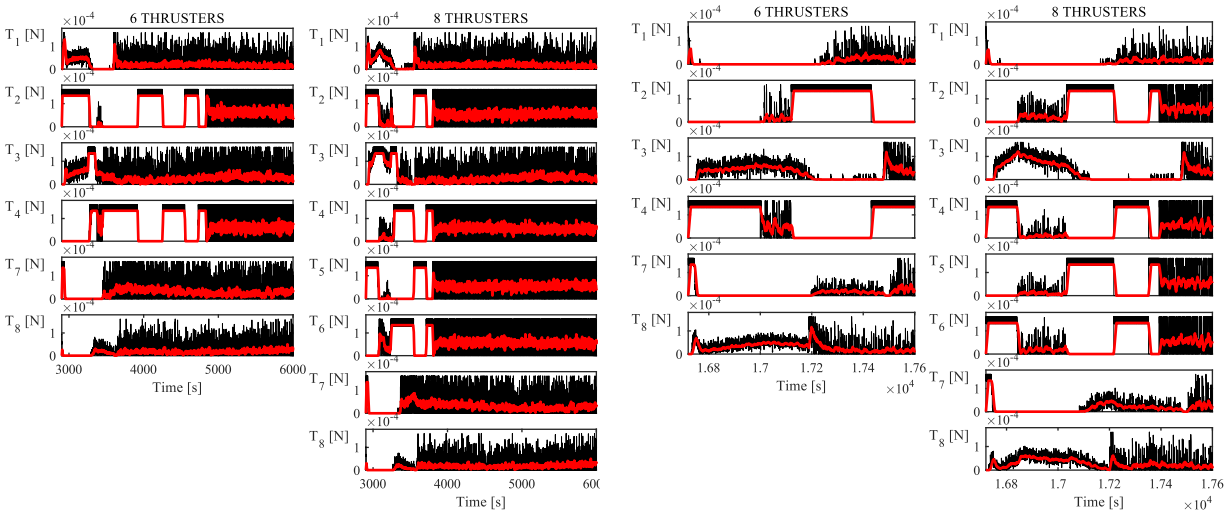

Figure 14: The effort of the thrusters considering the configuration with 6 and 8 pairs of emitters during sun-pointing modes (left) and communication modes (right)

moving average. In particular, it is possible to observe, during sun-pointing modes, that in both configurations, the thrusters that provide a moment in x_b are almost always on. The resulting performances of the two configurations in this phase are very similar, and therefore it would be beneficial to use fewer emitters.
In the communication mode, it must be ensured that one face of the spacecraft, the one where the antenna is located, always points toward the nadir. As in the previous mode, quaternions are shown in Figure. 13. A lower steady state error is noticed after an initial amount of time. The difference between the two configurations, on the other hand, is minimal. As in the thrust pointing mode and for the same reasons, the effort of the thrusters providing a moment in z_B is smaller (Figure. 14).
Considering the entire mission, which consists of 7 orbits, unlike the previous scenario, it is necessary to consider phase changes that, in the thrust pointing mode, cause an initial misalignment of the main thrust. In fact, as previously mentioned, the main thruster is turned on only during the thrust pointing phases. The propellant consumption in Figure. 15 shows that in the case of 6 pairs of emitters, almost 0.2 grams are saved. The dotted line, as in the previous scenario, indicates how much propellant would be necessary if the thrusters were always at maximum thrust. Also in this scenario, Figure. 15 shows a comparison with the position and the velocity ideal trajectory provided by 360^{TM} mission analysis tool. In this figure, it can be observed that a maximum position error of almost 200 meters, using 8 thrusters, is obtained. This error is due to the transition from one phase to the thrust phase and thus an initial oscillation that causes the thrust misalignment. Taking into account the configuration with 6 pairs of emitters, the error is greater because there are more oscillations and a longer rise time, as shown in Figure. 13, and thus a longer duration of misalignment.
The same outcomes can be observed by examining the classical orbital elements depicted in Figure. 16 when compared to the ideal case with perfect control (such as $\Delta i = i_{\text{ideal}} - i$). Although the 6 emitter configuration allows for propellant saving in the attitude actuation, the larger pointing error causes an increase of propellant mass needed from the main thruster to perform the maneuver and reach the final orbit, with a potential increase of maneuvering time as well.

DOI: 10.13009/EUCASS2023-989

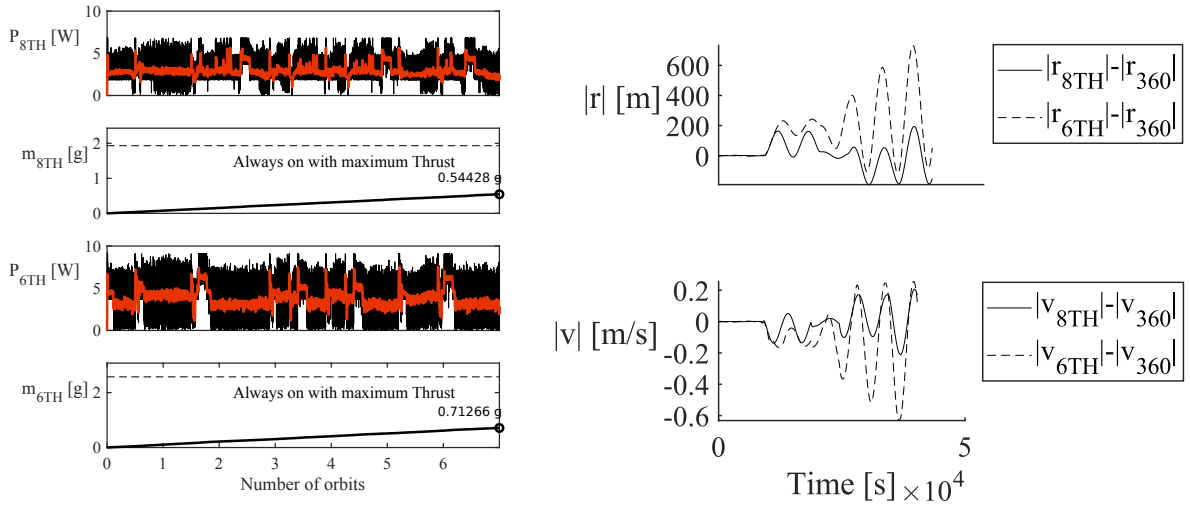

Figure 15: Propellant and total power consumption for both configurations during the entire mission (left). Shown in red is the moving average. Error in position and velocity compared with those provided by the 360^{TM} mission analysis tool (right)

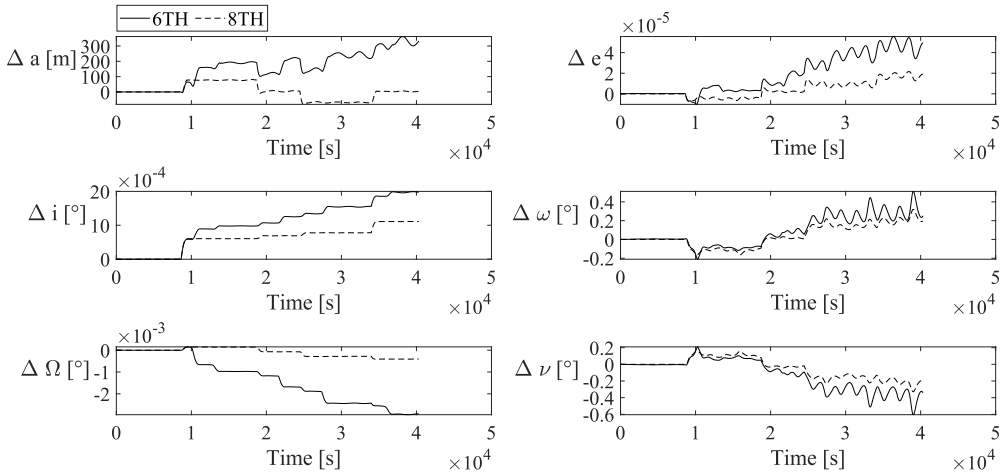

Figure 16: Classical orbital elements compared with the ideal case

5. Conclusions

This work address the problem of robust spacecraft attitude control with electrospray propulsion as attitude actuators, proposing a Dynamic Super Twisting Sliding Mode Control (DSTSMC) law technique. Two main objectives have been accomplished: achievement of adequate attitude control that would allow during the thrust pointing phase to achieve the predefined trajectory; and accomplishment of precise control during other mission phases, such as sun-pointing and communication. The other important task of this thesis was to investigate the effectiveness of ATHENA^{TM} electrospray as attitude actuators and evaluate their performance under different operating conditions.

The different configurations explored show that the thruster is capable of providing accurate torque with the control law applied even in the presence of external disturbances. In addition, an analysis of energy and propellant consumption was developed in order to explore the thrusters number and distribution, and define the most effective operating parameters. Variations in the physical properties of the spacecraft, such as its size and the integration of deployable solar panels, are also taken into account.

The results show the success of the suggested design and proposed controllers. In particular, it was seen that it is necessary to consider the number of emitter pairs depending on the phase and mission requirements: a smaller number

DOI: 10.13009/EUCASS2023-989

of emitter seems to allow for propellant and power saving, although the tracking performance is inferior, which might leads to increase of propellant need for the main thruster.
One of the key objectives for future investigations could be to achieve complete orbit and attitude control using only ATHENA^{TM} thrusters, combining the two functionalities in a single system. It will be necessary to confirm that the same control strategy tested in this study is adequate in order to achieve this, as well as to establish the ideal number and location of electrospray thrusters on a spacecraft to ensure optimal performance.
Moreover, there are various other operational modes that could be explored and tested to assess their efficiency and effectiveness. By continuing to push the boundaries of electrospray propulsion technology, we can gain valuable insights and develop new techniques that will ultimately lead to more sophisticated and capable spacecraft control systems.

References

[1] arcsec. *SAGITTA STAR TRACKER*. https://satsearch.co/products/arcsec-sagitta-star-tracker.

[2] Giulio Avanzini. Spacecraft attitude dynamics and control. *Politecnico di Torino*, 9:13, 2008.

[3] Honglong Chang, Liang Xue, Wei Qin, Guangmin Yuan, and Weizheng Yuan. An integrated mems gyroscope array with higher accuracy output. *Sensors*, 8(4):2886–2899, 2008.

[4] John L Crassidis, Srinivas R Vadali, and F Landis Markley. Optimal variable-structure control tracking of spacecraft maneuvers. *Journal of Guidance, Control, and Dynamics*, 23(3):564–566, 2000.

[5] Francisco de Borja De Saavedra, Brandon Israel Escamilla Estrada, and Daniel Perez Grande. Ienai go: A free tool for concurrent mission design and optimization with on-board electric propulsion. *73rd International Astronautical Congress (IAC)*, 2022.

[6] Giuseppe Di Pasquale, Daniel Peréz Grande, and Manuel Sanjurjo-Rivo. Space mobility optimization and concurrent engineering for modular micro-propulsion systems with 360 by ienai space. *73rd International Astronautical Congress (IAC)*, 2022.

[7] Mirko Leomanni. *Attitude and Orbit control techniques for spacecraft with electric propulsion*. PhD thesis, Ph. D. Dissertation, Dept. of Information Engineering and Mathematics, 2015.

[8] F Landis Markley and John L Crassidis. *Fundamentals of spacecraft attitude determination and control*, volume 1286. Springer, 2014.

[9] Fernando Mier-Hicks and Paulo C Lozano. Electrospray thrusters as precise attitude control actuators for small satellites. *Journal of Guidance, Control, and Dynamics*, 40(3):642–649, 2017.

[10] Yuri Shtessel, Christopher Edwards, Leonid Fridman, Arie Levant, et al. *Sliding mode control and observation*, volume 10. Springer, 2014.

[11] Silicon-Sensing. *CRH02-Angular Rate Sensor*. https://www.siliconsensing.com/media/1181/crh02-00-0100-132-rev-2.pdf.

[12] Martin N Sweeting. Modern small satellites-changing the economics of space. *Proceedings of the IEEE*, 106(3):343–361, 2018.

[13] Navin Timilsina. *Electrospray Thrusters for Attitude Control of a 1-U CubeSat*. University of California, Irvine, 2014.

[14] Jason Tuthill. Design and simulation of a nano-satellite attitude determination system. Technical report, Naval postgraduate school Monterey CA Dept of mechanical and Astronautical, 2009.

[15] D. Villegas, S. Correyero, M. Wijnen, and P. Fajardo. Indirect characterization of athena performance, a novel externally wetted electrospray propulsion system. *Space Propulsion 2022*, 2022.

[16] Michael JH Walker, B Ireland, and Joyce Owens. A set modified equinoctial orbit elements. *Celestial mechanics*, 36(4):409–419, 1985.